Supporting information for

Exceptional green hydrogen production performance with ruthenium modulated nickel selenide

Rong Li [a], Lanli Chen [c], Huaming Zhang [a*], Muhammad Humayun [b,d], Junhong Duan [a], Xuefei Xu [d], Yanjun Fu [a], Mohamed Bououdina [b], Chundong Wang [d,b*]

[a] Jiangxi Province Key Laboratory of Optoelectronic Information Science and Technology, Nanchang Hangkong University, Nanchang 330063, Jiangxi, China

[b] Energy, Water, and Environment Lab, College of Humanities and Sciences, Prince Sultan University, Riyadh 11586, Saudi Arabia

[c] School of Mathematics and Physics, Hubei Polytechnic University, Huangshi 435003, PR China

[d] School of Integrated Circuits, Wuhan National Laboratory for Optoelectronics, Huazhong University of Science and Technology, Wuhan 430074, P.R. China

Email: 70451@nchu.edu.cn (H.M. Zhang); apcdwang@hust.edu.cn (C.D. Wang)

Experimental section

Chemicals and materials: Se powder [Se, 99.9% metals basis], ethylene glycol [$HOCH_2CH_2OH$, ＞99%, GC], ethylenediamine [$C_2H_8N_2$, ＞99%], ruthenium trichloride ($RuCl_3 \cdot 3H_2O$, 97%), and iridium chloride hydrate ($IrCl_3 \cdot xH_2O$) were purchased from Aladdin Chemical Reagent Co., Ltd. (China). Potassium hydroxide (KOH), hydrochloric acid (HCl), acetone, and absolute ethanol were obtained from Shanghai Sinopharm Chemical Reagent Co., Ltd. Nickel foam (NF), with a thickness of 1.5 mm, bulk density of 0.29 g/cm^3, and pore number per inch of 120, was acquired from Kunshan Zhenyuhongxin Materials Co. Ltd. Platinum on activated carbon [20 wt% Pt/C] and Ruthenium(IV) Oxide [20 wt% RuO_2] was available from Sigma Aldrich Shanghai Trading Co., Ltd. and Aladdin Co., Ltd., respectively. The deionized (DI) water used in the experiments was purified in the laboratory via the Millipore system. All the reagents involved in this study were of analytically grade andemployed without further purification.

Preparation of Ni_3Se_2 on NF: First of all, the nickel foam was pretreated: a piece of nickel foam (NF, 2 × 2 cm^2) was successively ultrasonically cleaned with 3 M hydrochloric acid, absolute ethanol, acetone and deionized water (15 min each) to remove the oxide on the surface, and then the cleaned nickel foam was vacuum-dried for use. Ni_3Se_2 was grown NF using a simple one-step hydrothermal method: 0.032g of selenium powder was added to a mixed solution consisting of 20 mL of ethylene glycol and 40 mL of ethylenediamine, and magnetic stirring for 30 minutes to thoroughly stir the powder and solution. The homogeneous solution and pretreated NF were then placed in a 100 mL volume Teflon-lined autoclave, sealed and placed in an oven.

Set the reaction temperature to 160 °C and allow it to undergo hydrothermal reaction for 24 h. After the autoclave cooled down naturally to ambient temperature, the Ni foam was carefully removed from the reaction vessel, washed with deionized water and ethanol several times, and then dried in a vacuum oven at 60 ºC overnight.

Preparation of Ru/Ni_3Se_2 on NF: The Ru/Ni_3Se_2/NF was synthesized by a simple impregnation method. Add 0.01 g of $RuCl_3 \cdot 3H_2O$ in 10 mL of DI water, stir continuously for 10 minutes, and add a piece of Ni_3Se_2 to the solution at 25℃ for 4 h. Subsequently, the fabricated Ru/Ni_3Se_2 sample was collected and dried in vacuum at 60 ◦C overnight. For comparison, The Ni_3Se_2 was immersed in different concentrations of $RuCl_3$ aqueous solution: 0.5, 1, 1.5 or 2 mg mL^{-1} of $RuCl_3 \cdot 3H_2O$. After four hours of immersion, the samples were recorded as $Ru_{0.5}/Ni_3Se_2$, Ru_1/Ni_3Se_2, $Ru_{1.5}/Ni_3Se_2$ and Ru_2/Ni_3Se_2, respectively. We also studied the effects of different immersion time on sample properties. The Ni_3Se_2 nanowires precursor was etched by 1 mg mL^{-1} $RuCl_3$ aqueous solution with different time of 2, 4, and 6 h, and the corresponding samples were marked as Ru/Ni_3Se_2-2, Ru/Ni_3Se_2-4, and Ru/Ni_3Se_2-6.

Preparation of Ru/Ni_3Se_2 on carbon cloth (*CC*): The preparation of Ru/Ni_3Se_2/CC was similar to that of Ru/Ni_3Se_2/NF, except that NF was replaced with CC.

Preparation of Ir/Ni_3Se_2 on NF: The preparation of Ir/Ni_3Se_2 was similar to that of Ru/Ni_3Se_2, except that $RuCl_3 \cdot 3H_2O$ was replaced with $IrCl_3 \cdot xH_2O$.

Preparation of Pt/C andRu_2O on NF: The 20% Pt/C and RuO_2 electrodes were prepared using typical methods. In short, first disperse 20% Pt/C (5 mg) or RuO_2 (5 mg) in a solution of 0.8 mL deionized water, 1.08 mL anhydrous ethanol, and 0.12 mL of 5% Nafion solution. That mixture was then ultrasonicated for 30 min to form a homogeneous catalyst ink. 0.02 mL of ink was then loaded onto Ni foam (1×2 cm^2) by rotational deposition. After that, the sample was placed in an oven and dried for further testing.

Characterizations: Different analytical techniques were used to characterize the chemical composition and microstructure of the electrocatalyst. X-ray diffraction (XRD) patterns were collected on a Bruker D8 Advance X-ray diffractometer using Cu Kα radiation (λ = 1.5416 Å) with a 2θ scan range between 10° and 80°, and can be used to detect the phase composition of the samples. The morphology and microstructure of as-made catalysts were studied by scanning electron microscopy (SEM, Zeiss Gemini 300) and transmission electron microscopy (TEM, FEI Tecnai F20). High-resolution TEM (HR-TEM) and high angle annular-dark-field scanning TEM (HAADF−STEM) techniques were employed to further investigate the morphology, crystal structure and element composition of the electrocatalysts. X-ray photoelectron spectroscopy (XPS) measurements can be used to analyze the elemental chemical states of the catalyst materials, which were performed on a Thermo Kalpha X-ray photoelectron spectrometer with Mono Al Kα radiation at energy of about 1486.6 eV. The Ru contents were tested by Inductively Coupled Plasma-Mass Spectrometry (ICP-MS) technique (Aglient 7800).

Electrochemical Measurements: The electrochemical measurements were performed in a

standard three-electrode cell system by using a CHI 660E workstation (Chenhua, Shanghai, China) in 1 M KOH aqueous solution. The as fabricated materials were cut into 2 × 1 cm^2 size as the working electrodes, the graphite rods was used as the counter electrode, and Hg/HgO electrode was used as the reference electrode. Linear sweep voltammetry (LSV) tests of the electrocatalysts for polarization curves were performed at a scan rate of 5 mV s^{-1}, and for Tafel-plot measurements, a scan rate of 0.1 mV s^{-1} was used. All the polarization curves were corrected with a 85% IR compensation, and the measured potential was converted relative to RHE according to the following equation: $E_{(RHE)} = E_{(Hg/HgO)} + 0.059\ pH + 0.098$. The Tafel slope was calculated by fitting the linear portion of the Tafel plots, obtained using the Tafel equation ($\eta = b\log(j) + a$, where b represents the slope and j represents the current density). Based on the Tafel equations, the exchange current density (j_0) can be calculated. Electrochemical impedance spectroscopy (EIS) measurements were performed with the frequency range from 0.01 Hz to 100 kHz. The electrochemical double layer capacitance (C_{dl}) was determined with cyclic voltammetry (CV) measurements at various scan rates in nonreactive region. The C_{dl} was further used to obtain the electrochemical active surface area (ECSA) values according to the equation: $ECSA = C_{dl}/C_s$, where Cs is the specific capacitance value of an ideal flat surface with a real surface area of 1 $cm^{2,}$ and in this work take the general value of 60 μF cm^{-2} for C_s. The long-term stability was tested by a chronoamperometry method. The overall water splitting was conducted with a two-electrode system at scan rate of 5 mV s^{-1}.

Theoretical calculations: All the calculations were based on the density function theory (DFT) calculations implemented in the framework of the Vienna *ab-initio* simulation package (VASP).

The exchange-correlation function was utilized and generalized gradient approximation (GGA) with the Perdew-Burke-Ernzerhof (PBE). The valence electrons were treated explicitly with a plane-wave basis set at a cutoff energy of 450 eV. The geometric optimizations were ceased when the force and energy were declined below 0.02 eV/Å and 10^{-5} eV, respectively. The calculation of Ni_3Se_2 (001) slab model contained 15 Ni atoms and 10 Se atoms. A vacuum space of 20 Å was used. The formula for ΔE_{H^*} and ΔG_{H^*} of hydrogen adsorption on pristine Ni_3Se_2 (001) and Ru-doping Ni_3Se_2 (001) are described as follows: $\Delta E_{H^*} = E_{H^*Slab} - E_{Slab} - 1/2E_{H2}$ and $\Delta G_{H^*} = \Delta E_{H^*} + \Delta ZPE - T\Delta S$, where E_{H^*Slab} is the energy used for the adsorption of single hydrogen atoms, E_{Slab} is a pure surface energy, and E_{H2} is the energy of adsorbed hydrogen molecules.

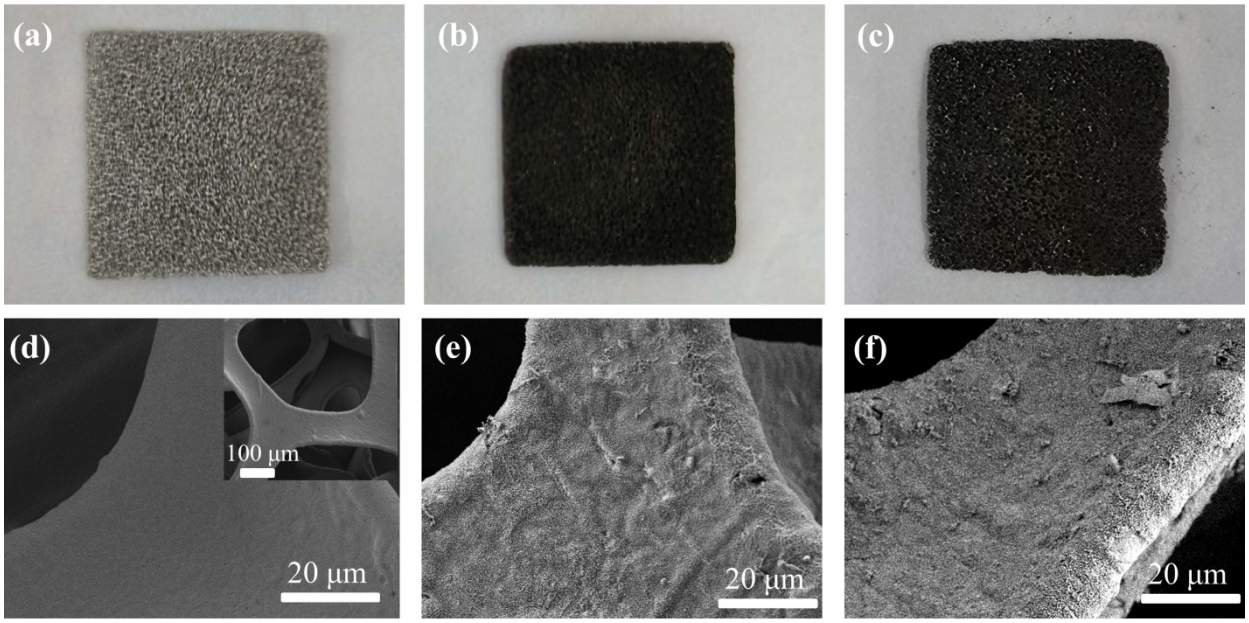

Figure S1. (a-c) are physical figures of NF, Ni_3Se_2 and Ru/Ni_3Se_2, respectively. (d-f) are SEM images for NF, Ni_3Se_2 and Ru/Ni_3Se_2, respectively.

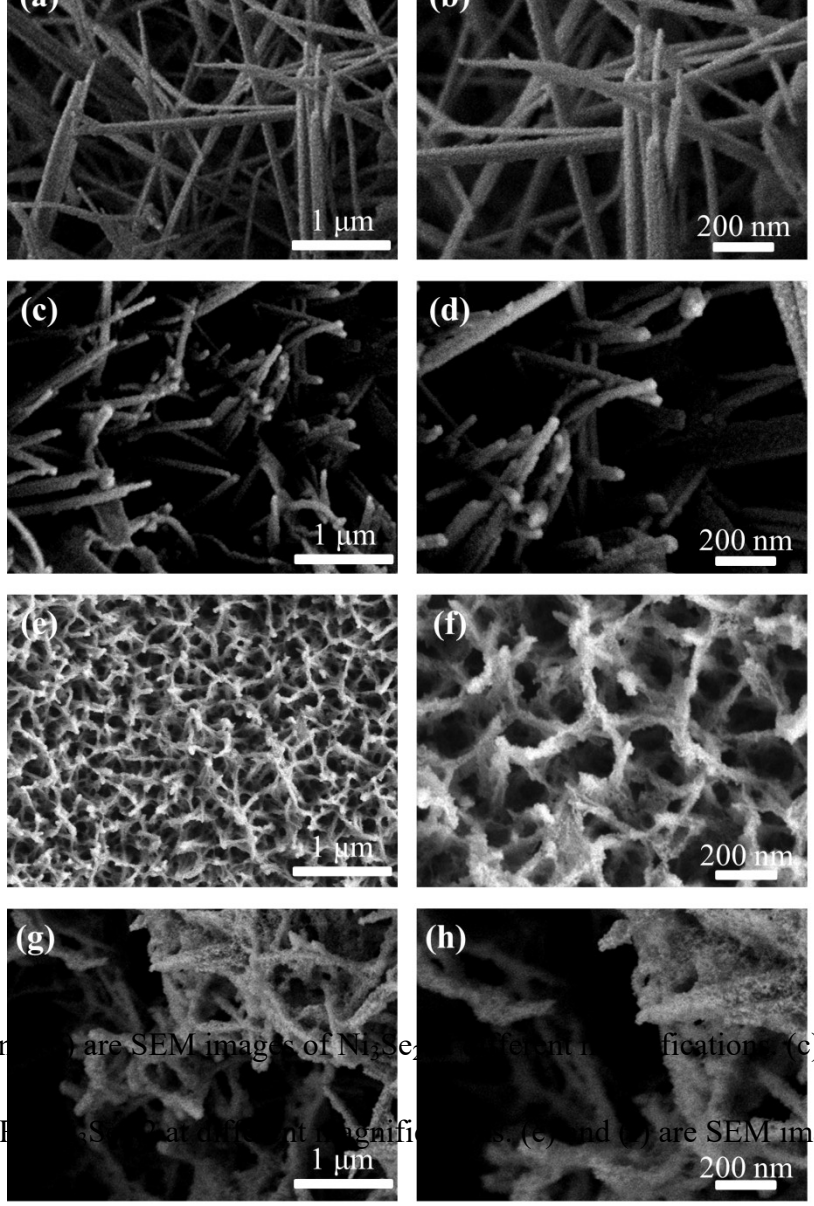

Figure S2. (a) and (b) are SEM images of Ni_3Se_2 at different magnifications. (c) and (d) are SEM images of Ru/Ni_3Se_2 at different magnifications. (e) and (f) are SEM images of Ru/Ni_3Se_2-4 at different magnifications. (g) and (h) are SEM images of Ru/Ni_3Se_2-6 at different magnifications.

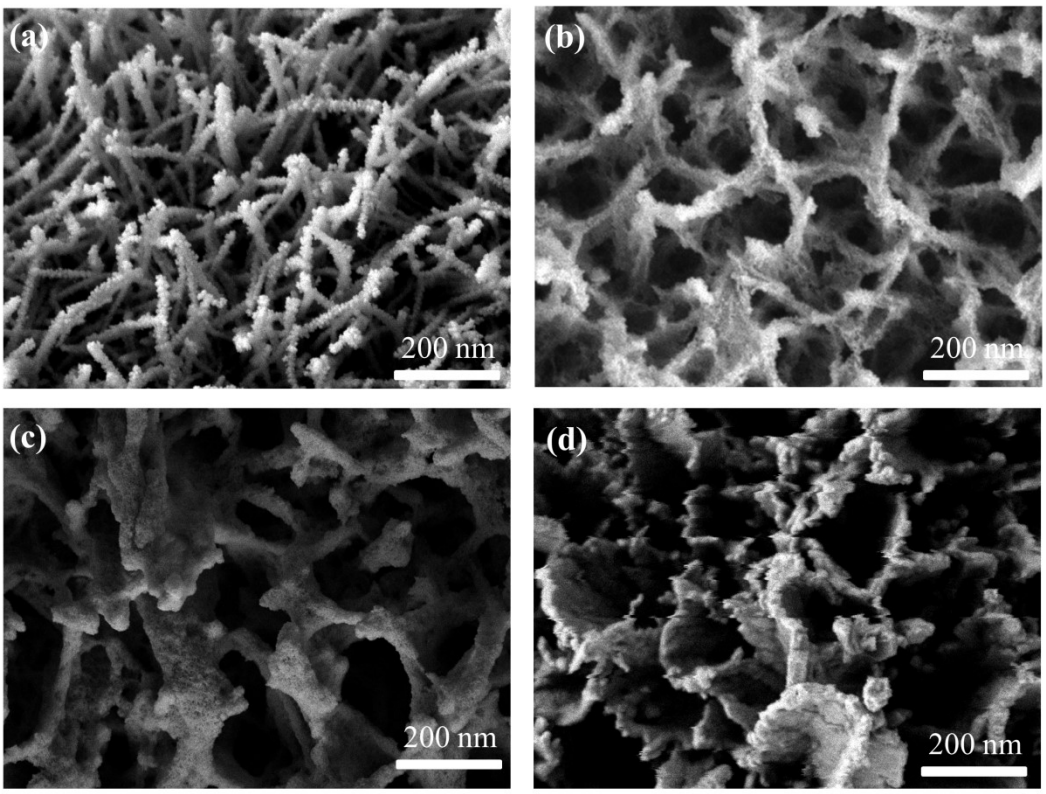

Figure S3. (a) SEM images of $Ru_{0.5}/Ni_3Se_2$, (b) SEM images of Ru_1/Ni_3Se_2, (b) SEM images of $Ru_{1.5}/Ni_3Se_2$, and (d) SEM images of Ru_2/Ni_3Se_2.

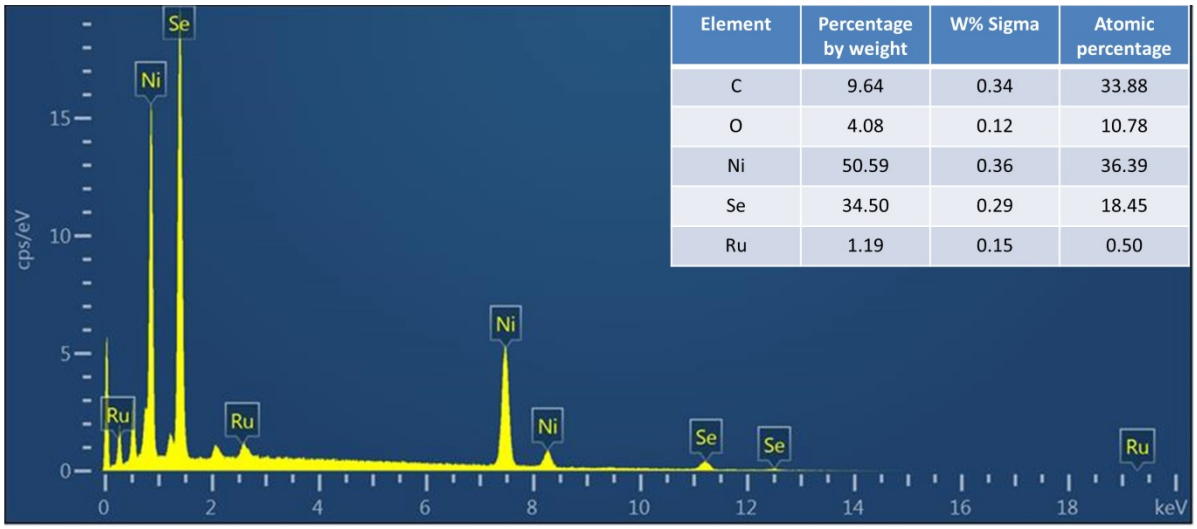

Element	Percentage by weight	W% Sigma	Atomic percentage
C	9.64	0.34	33.88
O	4.08	0.12	10.78
Ni	50.59	0.36	36.39
Se	34.50	0.29	18.45
Ru	1.19	0.15	0.50

Figure S4. EDS spectrum of Ru/Ni_3Se_2.

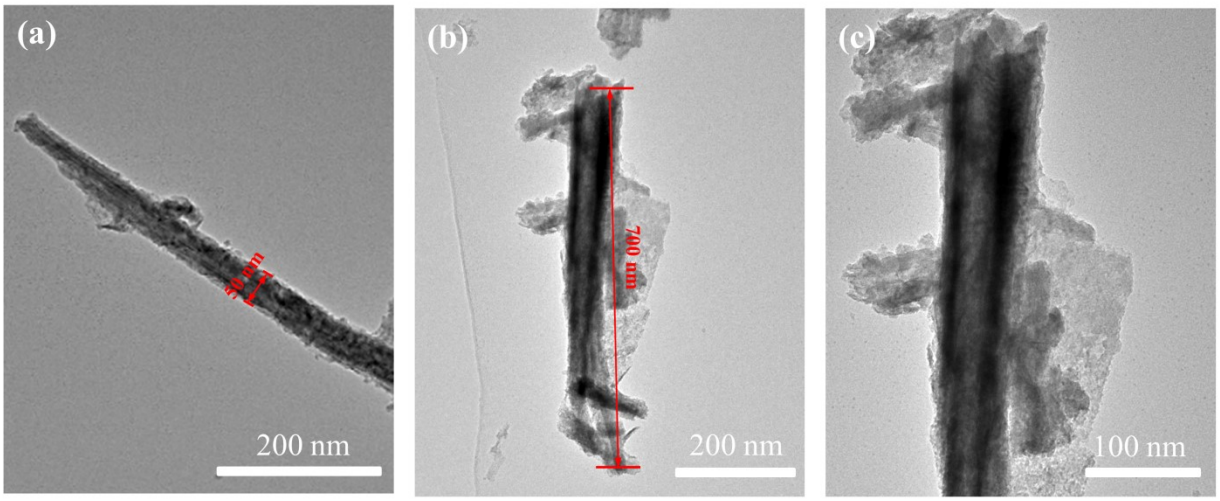

Figure S5. (a), (b), and (c) are TEM images of Ru/Ni_3Se_2 at different magnifications.

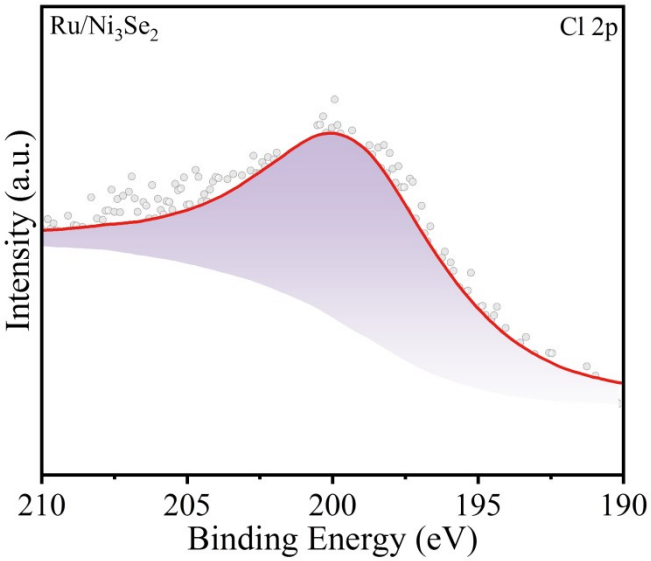

Figure S6. High-resolution XPS spectra of Cl 2p.

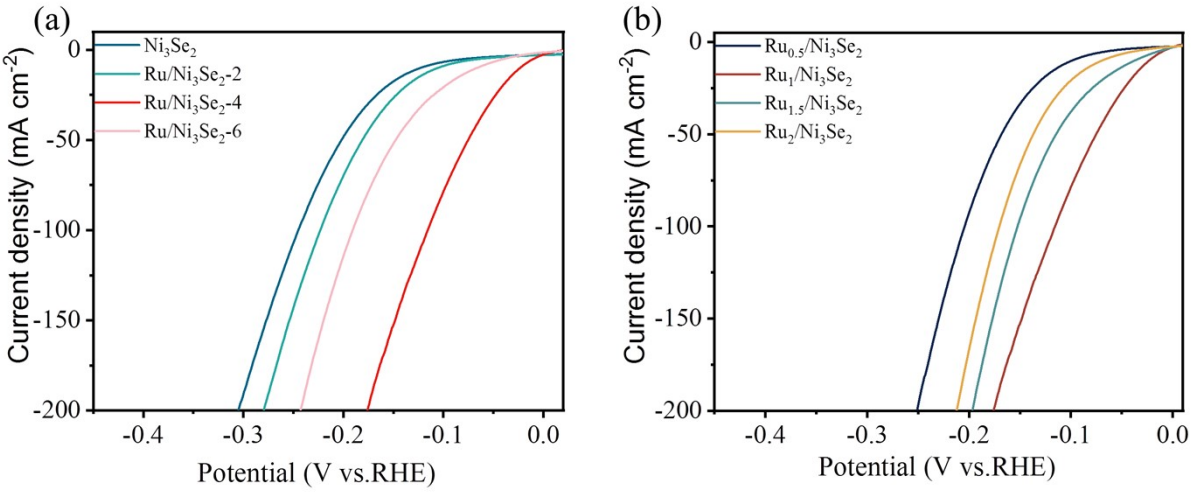

Figure S7. (a) Polarization curves of Ni_3Se_2 immersion in different time. (b) HER performance of Ru/Ni_3Se_2 with different $RuCl_3$ contents.

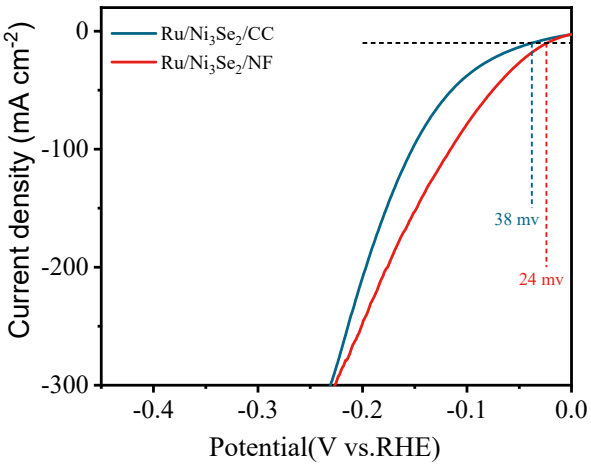

Figure S8. Electrocatalytic HER performances of $Ru/Ni_3Se_2/NF$ and $Ru/Ni_3Se_2/CC$ in 1 M KOH.

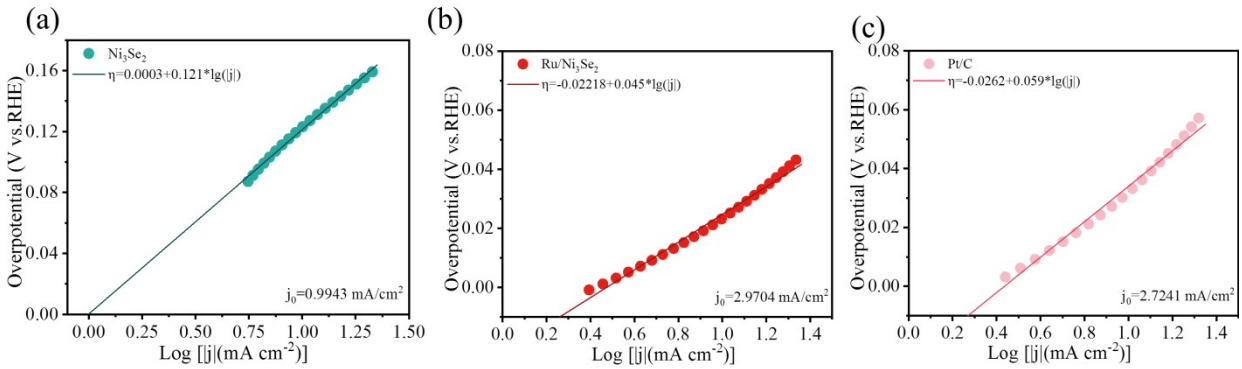

Figure S9. The exchange current densities for (a) Ni_3Se_2, (b) Ru/Ni_3Se_2 and (c) Pt/C by applying extrapolation method to the Tafel plots in 1 M KOH.

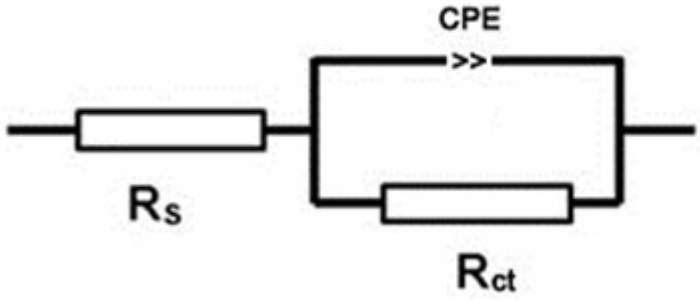

Figure S10. The corresponding equivalent circuits.

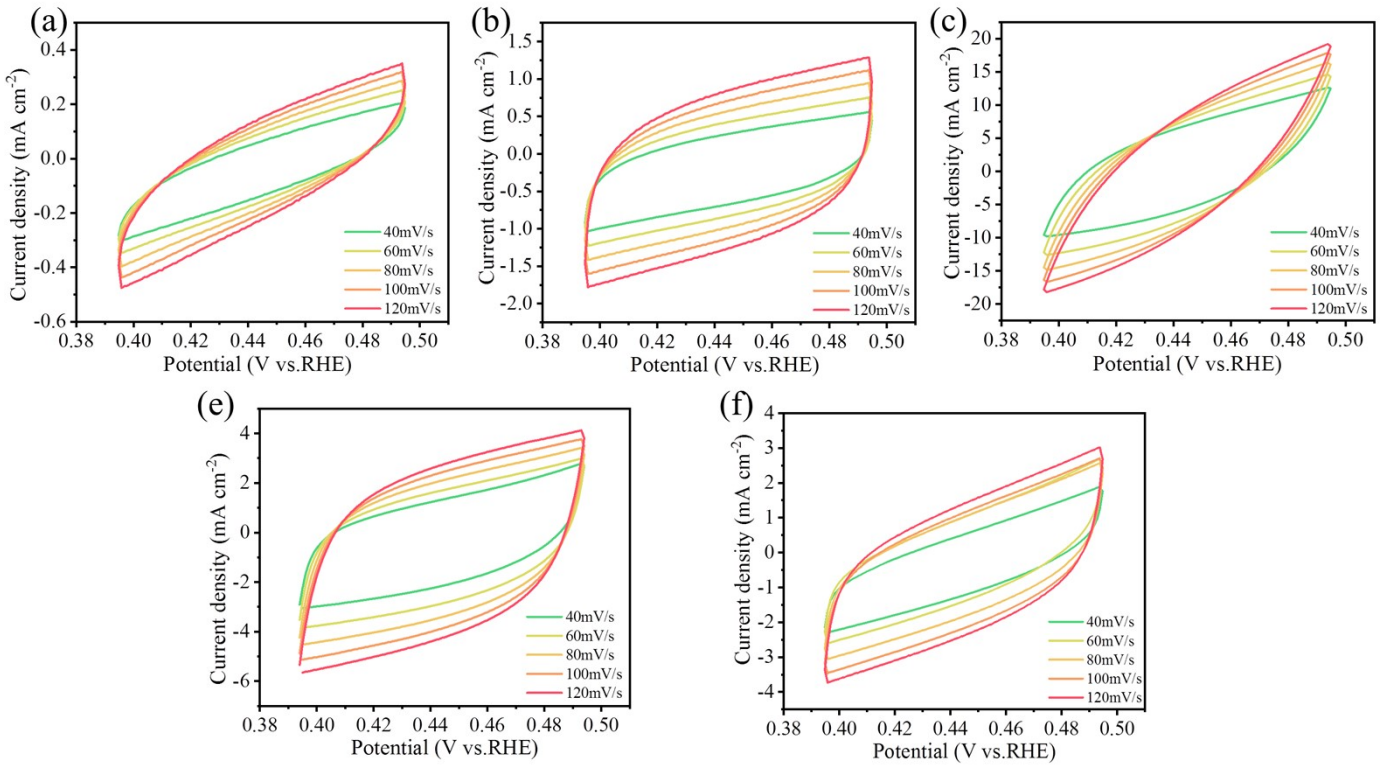

Figure S11. CV curves of the catalysts recorded in the region of 0.394 ~ 0.494 V *vs.* RHE at different scan rates. (a) NF, (b) Ni_3Se_2, (c) Ru/Ni_3Se_2, (d) Ir/Ni_3Se_2, (e) Pt/C.

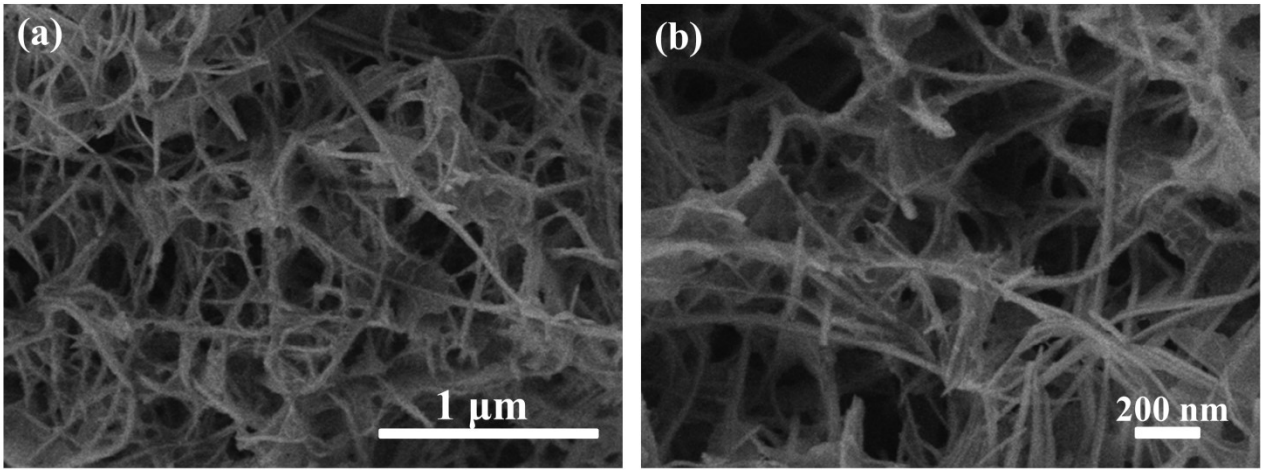

Figure S12. (a) and (b) SEM images of Ru/Ni_3Se_2 after HER stability test at different magnifications.

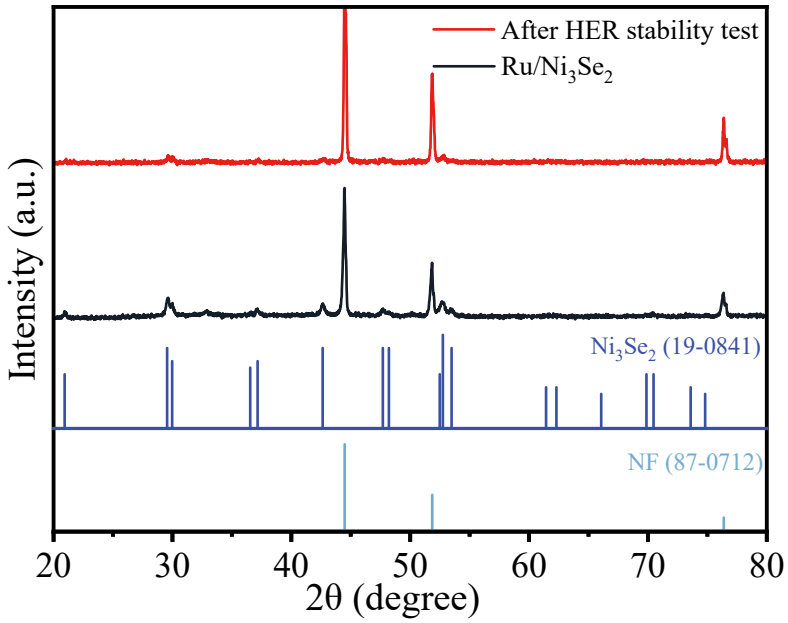

Figure S13. XRD patterns of Ru/Ni_3Se_2 after and before HER stability test.

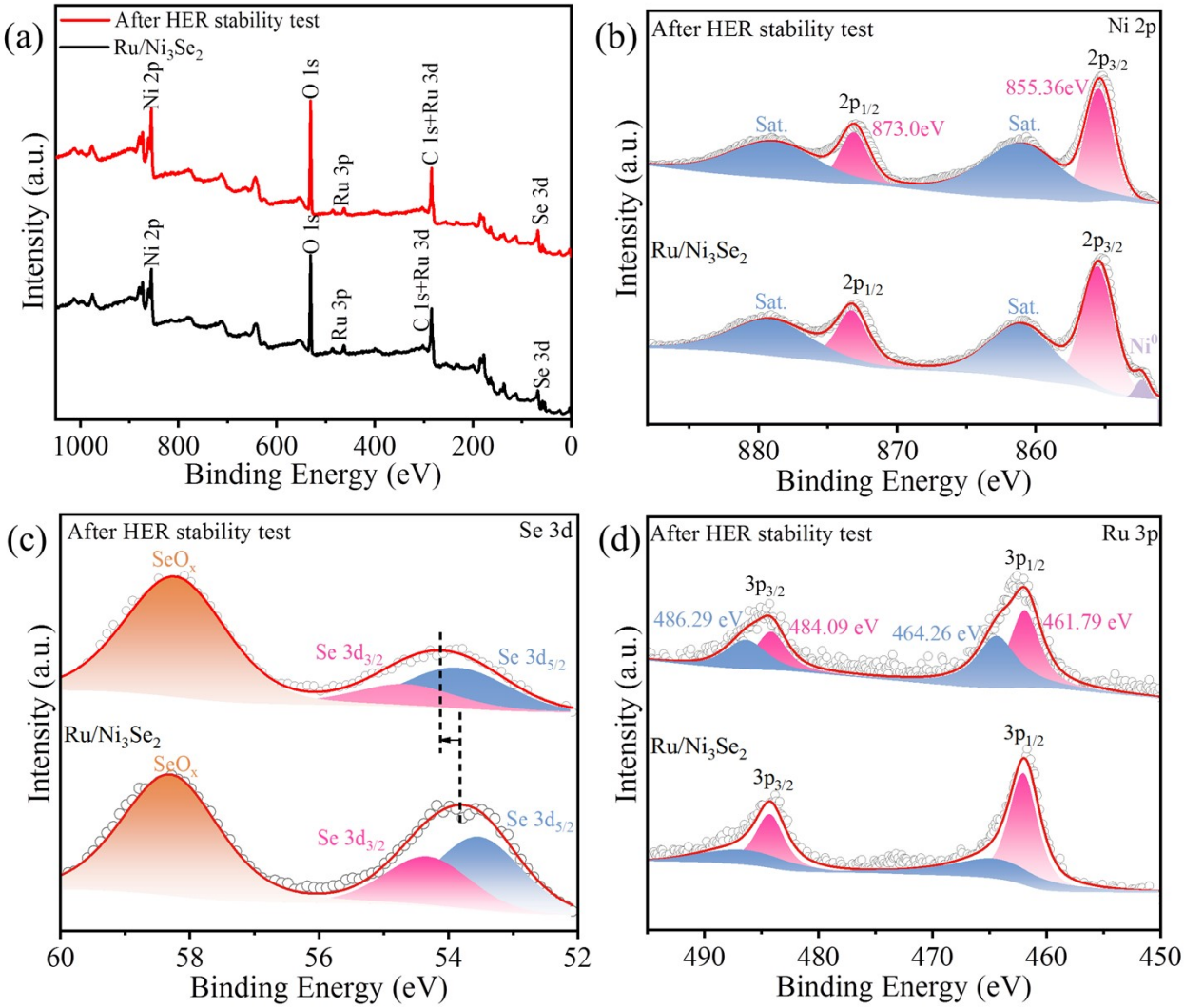

Figure S14. XPS spectrum analysis. (a) XPS survey spectra of Ru/Ni_3Se_2 before and after HER stability test. (b), (c) and (d) are the high-resolution Ni 2p, Se 3d and Ru 3p XPS spectra of Ru/Ni_3Se_2 before and after HER stability test.

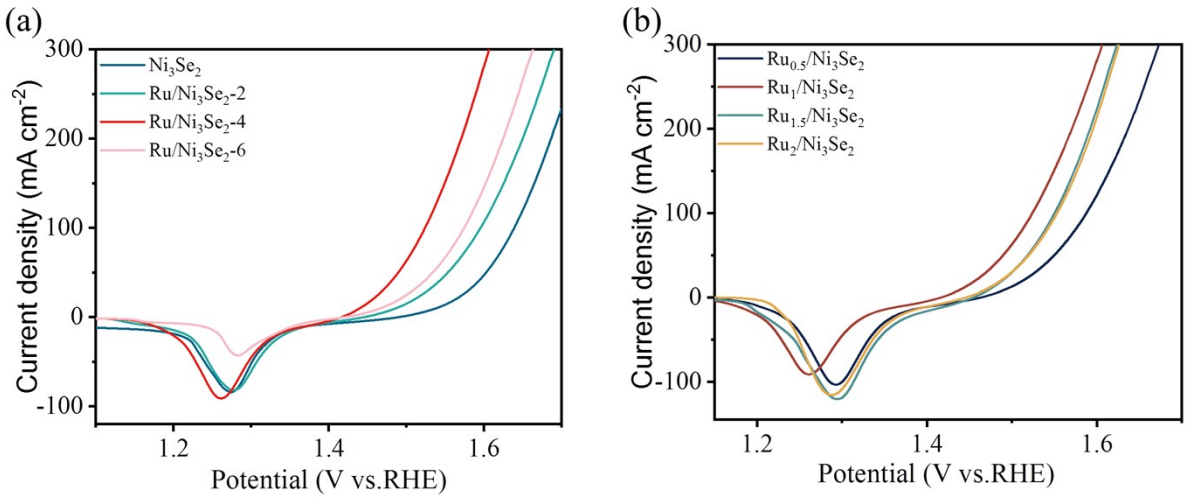

Figure S15. (a) Polarization curves of Ni_3Se_2 immersion in different time. (b) OER performance of Ru/Ni_3Se_2 with different $RuCl_3$ contents.

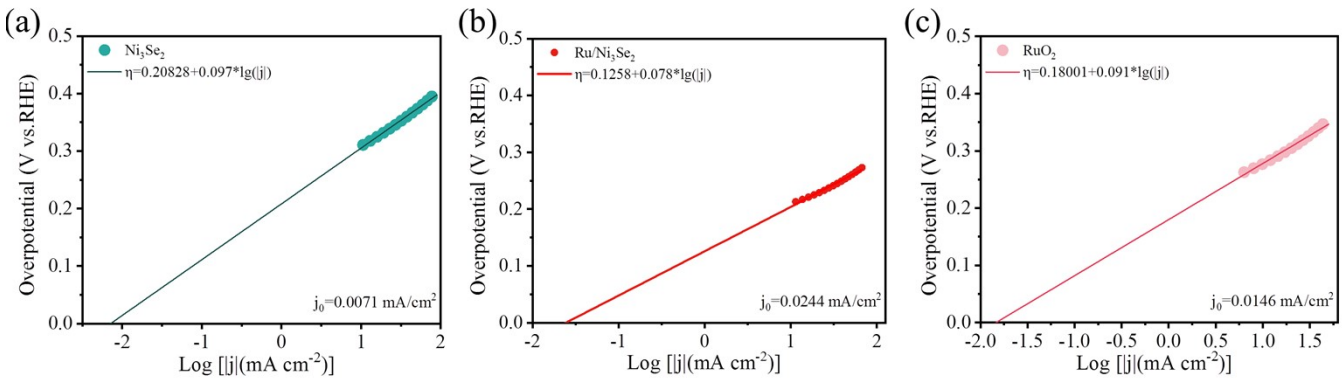

Figure S16. The exchange current densities for (a) Ni_3Se_2, (b) Ru/Ni_3Se_2 and (c) RuO_2 by applying extrapolation method to the Tafel plots in 1 M KOH.

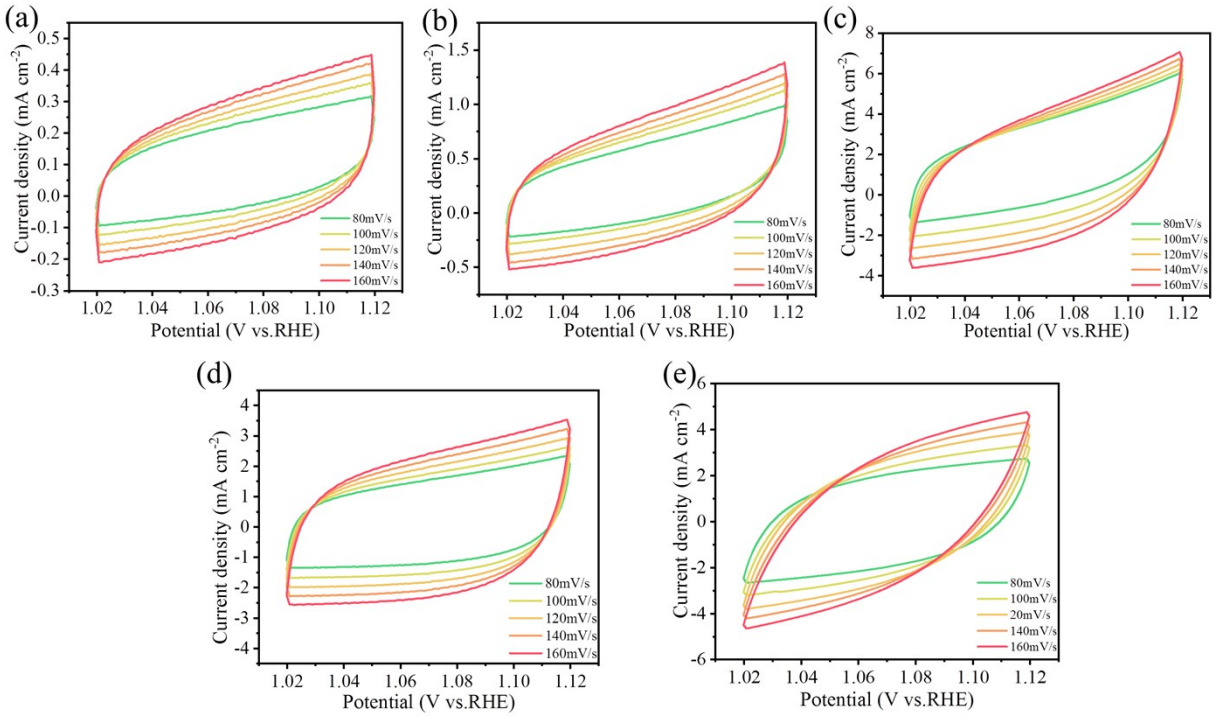

Figure S17. CV curves of the catalysts recorded in the region of 1.02 ~ 1.12 V *vs.* RHE at different scan rates. (a) NF, (b) Ni_3Se_2, (c) Ru/Ni_3Se_2, (d) Ir/Ni_3Se_2, (e) Pt/C.

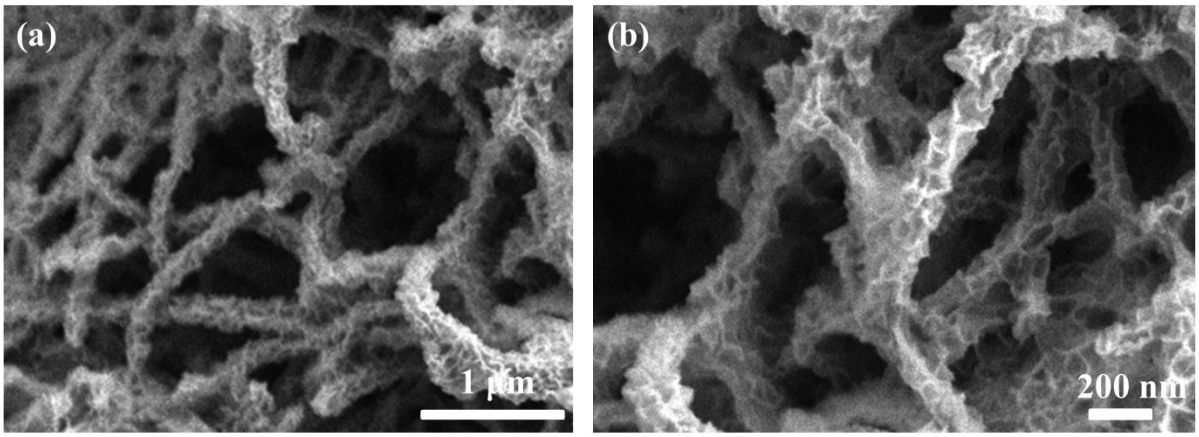

Figure S18. (a) and (b) SEM images of Ru/Ni_3Se_2 after OER stability test at different magnifications.

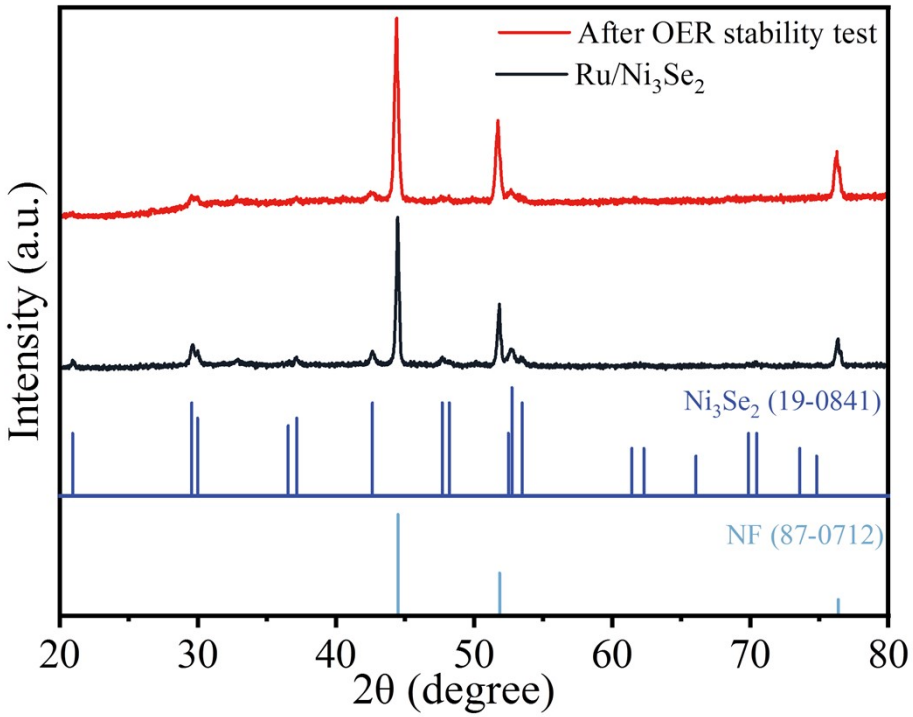

Figure S19. XRD patterns of Ru/Ni_3Se_2 after and before OER stability test.

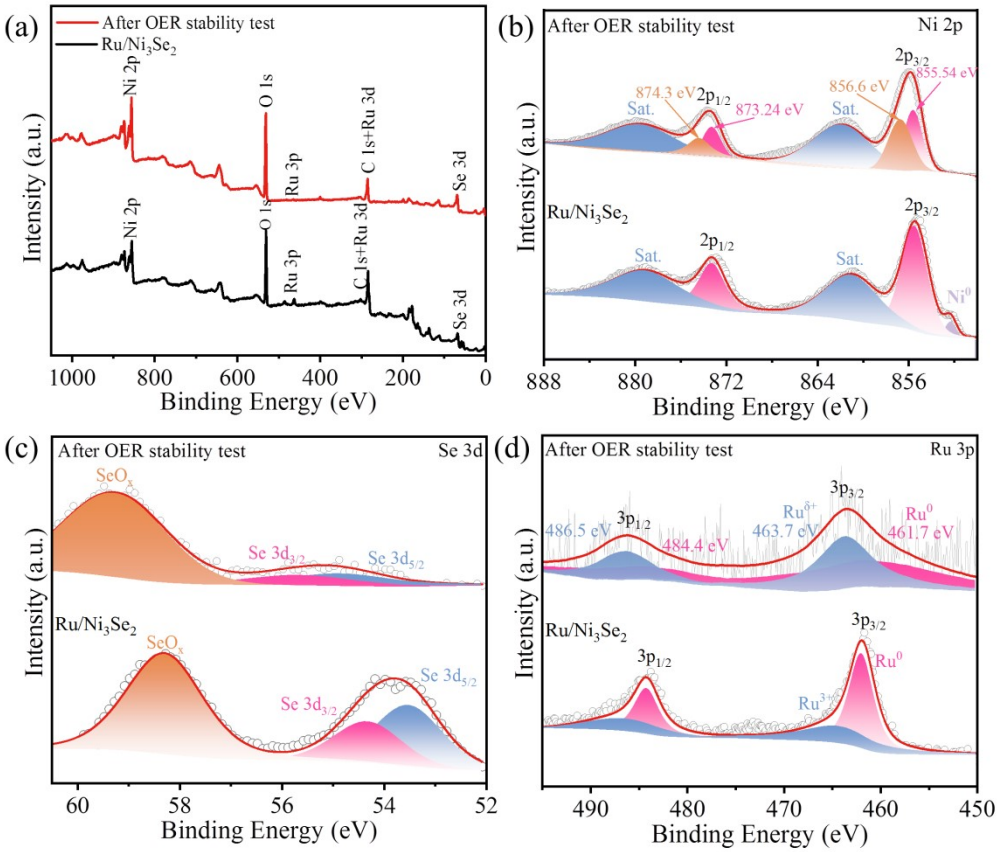

Figure S20. XPS spectrum analysis. (a) XPS survey spectra of Ru/Ni_3Se_2 before and after OER stability test. (b), (c) and (d) are the high-resolution Ni 2p, Se 3d and Ru 3p XPS spectra of Ru/Ni_3Se_2 before and after OER stability test.

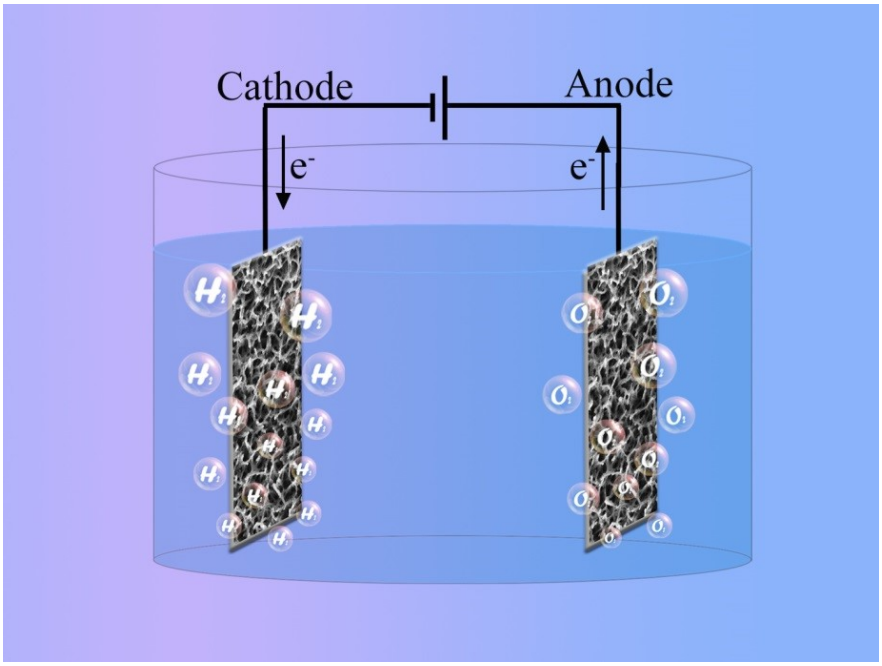

Figure S21. Schematic diagram of a two-electrode electrolyzer.

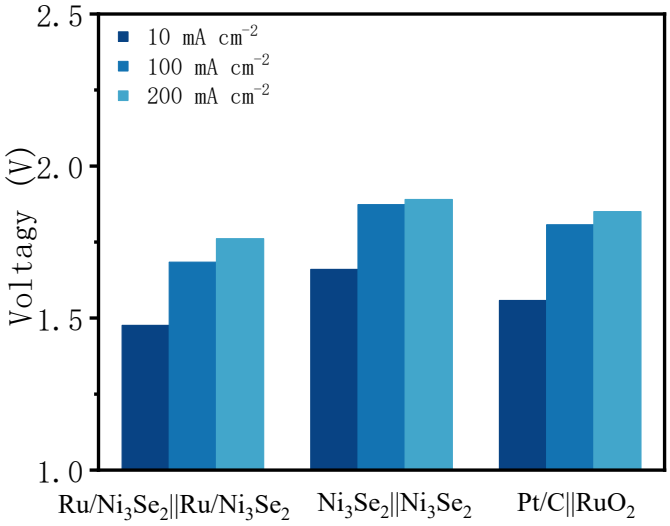

Figure S22. Comparison of overpotential of as-prepared catalysts at different current densities (η=10, 100, 200 mA cm^{-2}).

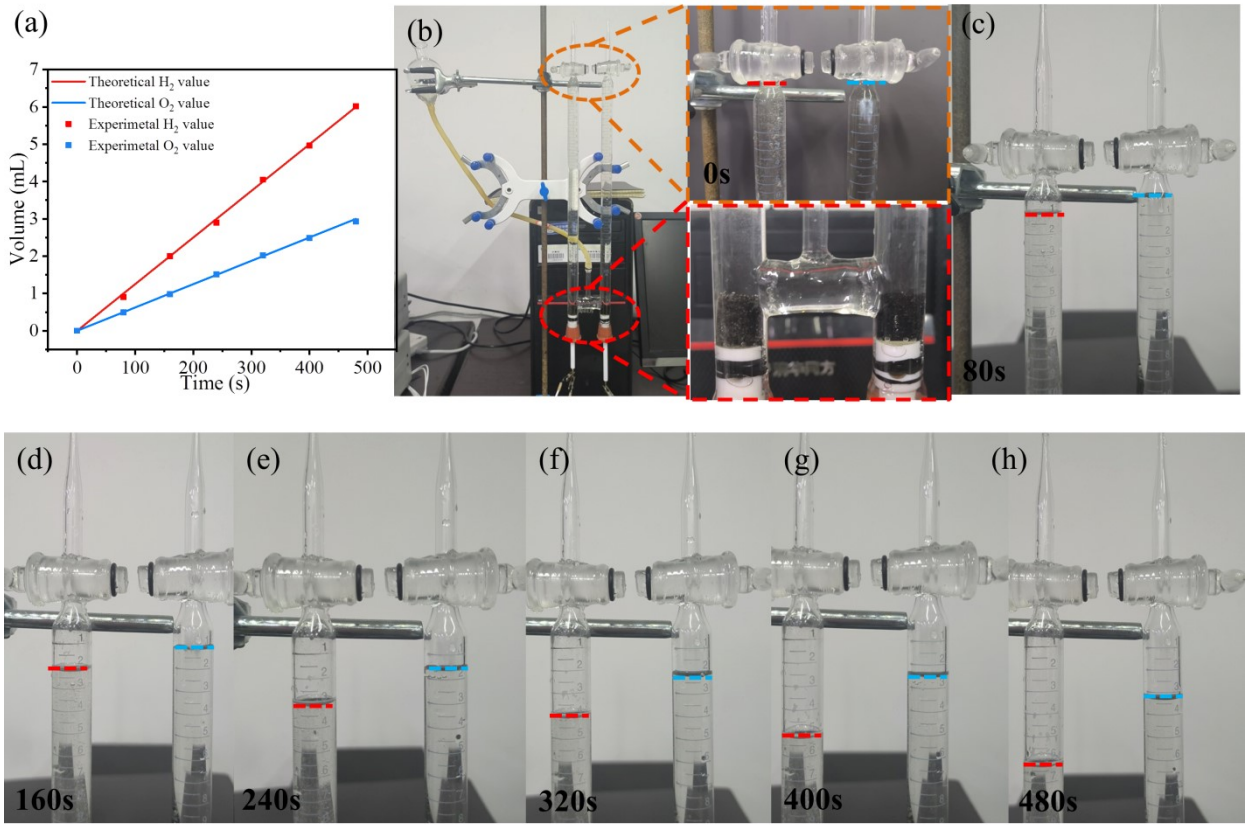

Figure S23. The overall water splitting performances in 1 M KOH. (a) Diagram of the amount of H_2 and O_2 released over time in 1 M KOH. (b) Device diagram for measuring Faraday efficiency. (c-h) Corresponding levels of H_2 and O_2 gases generated at different times 1 M KOH electrolyzer.

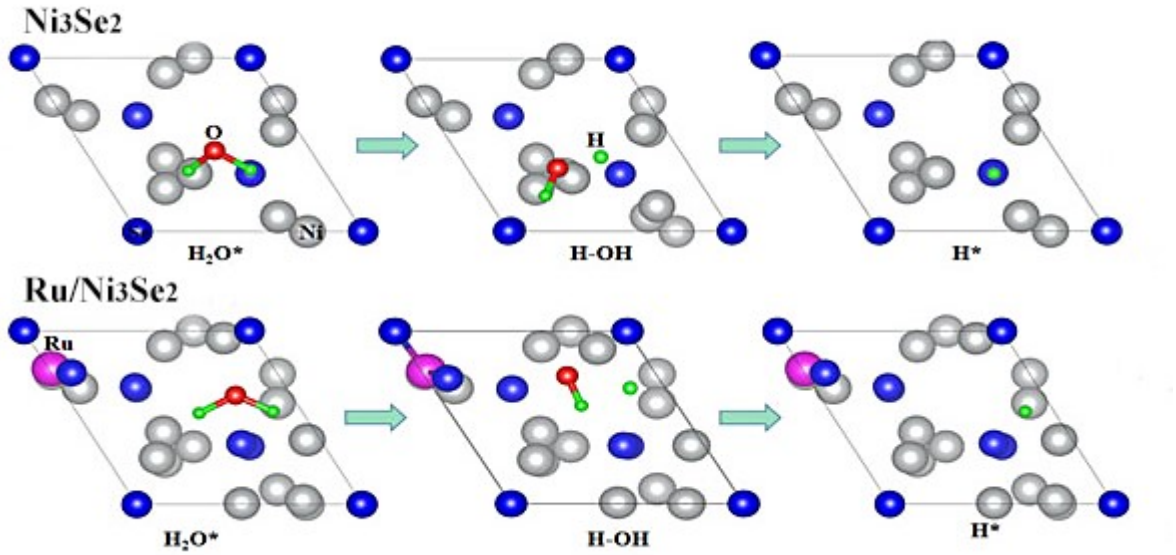

Figure S24. The top views of schematic models of water dissociation on the surfaces of Ni_3Se_2 (001) and Ru/Ni_3Se_2 (001) catalysts.

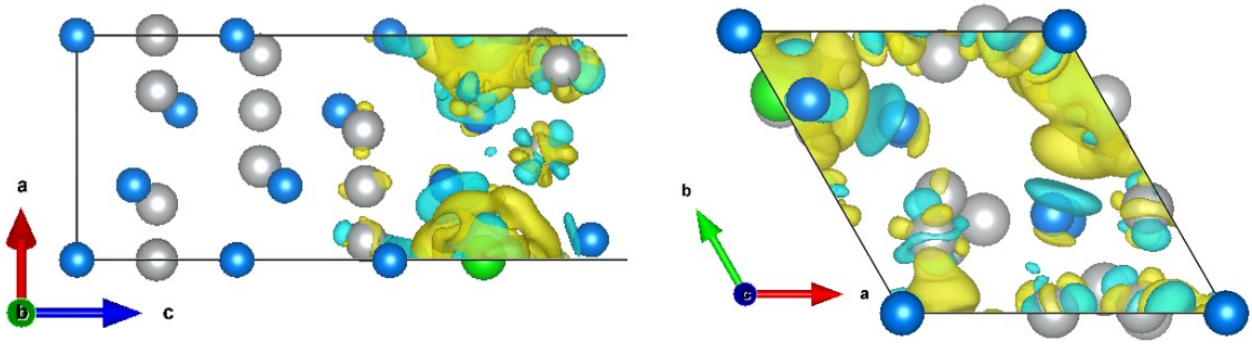

Figure S25. The difference charge density of $Ru/Ni_3Se_2(001)$. The isosurfaces value is 0.00377406 e/Å^3.

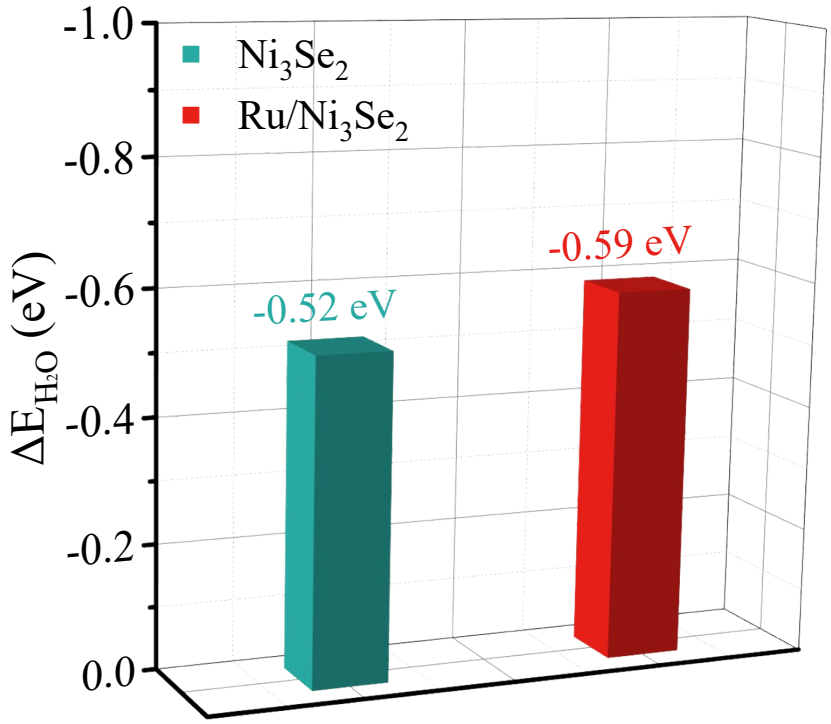

Figure S26. Calculated H_2O adsorption energy.

Table S1. The actual atomic percentage (wt%) of Ru elements in the Ru_Y/Ni_3Se_2 determined by ICP-MS.

Samples	$Ru_{0.5}/Ni_3Se_2$	Ru_1/Ni_3Se_2	$Ru_{1.5}/Ni_3Se_2$	Ru_2/Ni_3Se_2
Ru (wt %)	1.53	2.34	3.06	4.12

The Ru element adopts the ICP-MS method, and the instrument model is Aglient 7800. The data calculation formula is as follows:

$$C_x(mg/kg) = \frac{C_0(mg/L) * f * V_0(mL) * 10^{-3}}{m(g) * 10^{-3}} = \frac{C_1(mg/L) * V_0(mL) * 10^{-3}}{m(g) * 10^{-3}} \quad (1)$$

$$W(\%) = \frac{C_x(mg/kg)}{10^6} * 100\% \quad (2)$$

Among them, *m* is the mass of the sample taken when analyzing the sample; V_0 is the volume of the fixed volume after sample digestion, *f* is the dilution factor; C_o is the concentration of the test solution element; C_1 is the element concentration of the sample digestant stock solution; C_x is the final test result of the measured element; *W(%)* is the final test result of the measured element, expressed as a percentage, calculated by the above formula (2), corresponding to the data in the table.

Table S2. Electrocatalytic activity of HER and OER for the reported various electrocatalysts in 1 M KOH at the current density of 10 mA/cm^2.

Catalysts	HER		OER		References
	η (mV) @j (mA/cm^2)	Tafel Slope (mV/dec)	η (mV) @j (mA/cm^2)	Tafel Slope (mV/dec)	
Ru/Ni_3Se_2	24@10	45	211@10	85	This work
Ru-NiCoP/NF	44@10	45.4	216@20	84.5	1
Ru-Co_3O_4/CoP/TM	47@10	93	293@10	86.4	2
Ru-Ni_3N@NC	43@10	70	270@10	46	3
RuO_2-Fe_2O_3	148@10	43	292@10	56.08	4
Ru-NiFe LDH-F/NF	115.6@10	125.1	230@10	58.6	5
Ru (0.2)-NC	72.8@10	74	300@10	62	6
RuCo@C	91@10	106	230@10	110	7
Ni_3Se_2@ NiFe-LDH/NF	68@10	106.2	222@10	61.3	8
Ni_3Se_2@FeOOH/NF	87@10	86.4	224@10	55.2	9
NiSe/Ni_3Se_2/NF	92@10	101.2	260@20	69.2	10
V-Ni_3Se_2/NF	191@100	83	320@100	62	11
Ni_3S_2@NGCLs/NF	134@10	84	271@10	99	12
VS_4/Ni_3S_2-4F/NF	91@10	183.4	240@10	71.97	13
Ni_3S_2-NiO_x/NF	104@10	64	241@10	59	14
MoS_2/Ni_3S_2@CA	96@10	61	229@10	47	15

References

1. D. Chen, R. Lu, Z. Pu, J. Zhu, H.-W. Li, F. Liu, S. Hu, X. Luo, J. Wu, Y. Zhao and S. Mu, *Appl, Cata., B*, 2020, **279**, 119396.
2. K. Zhang, W. Ma, G. Tan, Z. Cheng, Y. Ma, W. Li, X. Feng and Z. Li, *Mol. Catal.*, 2022, **530**, 112640.
3. Y. Liu, D. Zheng, Y. Zhao, P. Shen, Y. Du, W. Xiao, Y. Du, Y. Fu, Z. Wu and L. Wang, *Int. J. Hydrogen Energy*, 2022, **47**, 25081-25089.
4. H. Mosallaei, H. Hadadzadeh, A. Foelske, M. Sauer, H. Amiri Rudbari and O. Blacque, *Dalton Trans.*, 2022, **51**, 6314-6331.
5. Y. Wang, P. Zheng, M. Li, Y. Li, X. Zhang, J. Chen, X. Fang, Y. Liu, X. Yuan, X. Dai and H. Wang, *Nanoscale*, 2020, **12**, 9669-9679.
6. Z. Yu, C. Si, F. J. Escobar-Bedia, A. P. LaGrow, J. Xu, M. J. Sabater, I. Amorim, A. Araujo, J. P. S. Sousa, L. Meng, J. L. Faria, P. Concepcion, B. Li and L. Liu, *Inorg. Chem. Front.*, 2022, **9**, 4142-4150.
7. C. Xu, X. Yang, X. Wen, Y.-Y. Wang, Y. Sun, B. Xu and C. Li, *CrystEngComm*, 2022, **24**, 4208-4214.
8. J. Hu, S. Zhu, Y. Liang, S. Wu, Z. Li, S. Luo and Z. Cui, *J. Colloid Interface Sci.*, 2021, **587**, 79-89.
9. J. Gao, H. Ma, L. Zhang, X. Luo and L. Yu, *J. Alloys Compd.*, 2022, **893**, 162244.
10. F. Zhang, Y. Pei, Y. Ge, H. Chu, S. Craig, P. Dong, J. Cao, P. M. Ajayan, M. Ye and J. Shen, *Adv. Mater. Interfaces*, 2018, **5**, 1701507.
11. D. He, L. Cao, J. Huang, Y. Feng, G. Li, D. Yang, Q. Huang and L. Feng, *ACS*

Sustainable Chem. Eng., 2021, **9**, 12005-12016.

12. B. Li, Z. Li, Q. Pang and J. Z. Zhang, *Chem. Eng. J.*, 2020, **401**, 126045.

13. L. Yaxin, C. Mingyuan, S. Na, H. Xingquan and C. Lili, *J. Electroanal. Chem.*, 2022, **927**, 116979.

14. Z. Huang, L. He, W. Zhang, W. Huang, Q. Mo, L. Yang, Q. Fu and Q. Gao, *J. Colloid Interface Sci.*, 2022, **622**, 728-737.

15. B. Zhang, H. Luo, B. Ai, Q. Gou, J. Deng, J. Wang, Y. Zheng, J. Xiao and M. Li, *Small*, 2023, **19**, e2205431.